Rate-Controlled Porosimetry: A State-of-the-Art Review

Jeffrey K. Daniels[1]*, Michael T. Myers[1], Lori A. Hathon[1]

[1]Department of Petroleum Engineering, University of Houston, Houston, Texas, USA

*Corresponding author; email: jkdaniels2@uh.edu

Abstract

Rate-controlled porosimetry is a powerful technique for studying the pore structure of porous media and the physical properties of porous media. This technique involves injecting and extracting a non-wetting fluid at a controlled rate into and from a porous medium, resulting in a fluctuating capillary pressure trace as a function of the injected non-wetting fluid volume. This review introduces the state-of-the-art rate-controlled porosimeters and techniques for studying geological porous media and the advancements made in our understanding of rate-controlled immiscible displacement processes. The insights gained from these studies are synthesized to facilitate cross-disciplinary research into the influence of pore structure on the petrophysical properties of geological porous media. Applications include enhanced oil recovery, site characterization for geological CO_2 storage, assessing the integrity of engineered barrier systems for safe nuclear waste disposal, and improving pore-scale models.

Introduction

The pore structure of geological porous media (porosity, pore body, throat size distribution, pore shape, pore connectivity, pore surface roughness) significantly influences their petrophysical properties. These properties are of key interest because they govern the estimated ultimate recovery (EUR) of hydrocarbons, capillary trapping of sequestered CO_2, and barrier integrity for underground nuclear waste disposal. Therefore, comprehensive pore structure characterization of geological porous media is essential to model fluid and transport properties and predict reservoir behavior accurately. Routine core analysis (RCAL) and special core analysis (SCAL/SPCAN) measurements are performed in the laboratory on core plugs retrieved from reservoir rocks to characterize pore structure. Capillary pressure measurements can be obtained by porous plate (Welge and Bruce, 1947), centrifuge (Donaldson et al., 1980), or mercury injection (Purcell, 1949) methods which are included in SCAL/SPCAN measurements. These methods can be categorized under pressure-controlled porosimetry. This experimental technique involves forcing non-wetting liquid into a core plug sample at successive pressure increments to characterize its pore structure. Mercury is mostly the non-wetting fluid of choice, but liquid Wood's metal and Field's metal are alternatives.

Mercury Injection Capillary Pressure (MICP) is the most widely used pressure-controlled porosimetry technique because it is quick and cost-effective compared to porous plate and centrifuge capillary pressure techniques and has been used to characterize the pore space of porous media since 1940 when Henderson et al. used this technique introduced by Washburn (1921a), to determine pore throat size distributions (van Brakel et al., 1981). The intrusion of mercury (a highly non-wetting substance) into the pore space of a porous medium is

possible when the pressure at the mercury interface is greater than the pressure of the wetting fluid in the porous medium (usually air in this porosimetry technique). The pressure difference across the interface of these two immiscible fluids is termed the capillary pressure. The pressure in the non-wetting phase is increased in successive steps to immiscibly the wetting phase until the non-wetting phase has either occupied the entire pore space or the pressure limit of the measurement apparatus is reached. The capillary pressure is recorded and plotted as a function of the cumulative volume of the non-wetting phase injected into the pore space. This pressure-volume data comprises a capillary pressure curve and is used with a pore space model to characterize the sample's pore space. This technique's non-wetting fluid should be non-reactive with the porous medium. Van Brakel et al. (1981) and Modrý et al. (1981) provide an excellent review of mercury injection porosimetry techniques and models for interpreting mercury porosimetry data. However, MICP only provides partial pore structure information (i.e., the pore throat size distribution) of porous media, which introduces some ambiguity in the pore structure information available from MICP capillary pressure curves since it is possible for porous media with different pore structures (due to a difference in pore body size distributions) to have similar capillary pressure curves. MICP combined with Nuclear Magnetic Resonance (NMR) or gas sorption to provide pore body size distributions eliminates some of these issues. Rock images may then be used to obtain information on pore topology for comprehensive pore structure characterization (Ruzyla, 1986).

Rate-controlled porosimetry is an alternative method that overcomes the limitations of traditional porosimetry techniques and is capable of providing comprehensive pore geometry (pore throats and the pore bodies they interconnect) information at multiple pore size ranges per the classification of Choquette and Pray (1970). This technique was pioneered by Yuan and Swanson (1989) using the Apparatus for Pore Examination (APEX), which injects a non-wetting fluid at a controlled low-capillary number ($N_{CA} \leq 10^{-5}$) flow rate into the pore space of a rock sample. As the pore space is intruded, the variation of the non-wetting fluid interface curvature results in a fluctuating capillary pressure trace as a function of the pore volume intruded. While rate-controlled porosimetry provides information on both pore bodies and the throats that interconnect them and insights into immiscible displacement processes, the technique is seldom employed as part of a core analysis program. There is, therefore, a dearth of literature regarding this technique compared to conventional pressure-controlled porosimetry.

Rate-controlled porosimetry also has applications in characterizing polymer electrolyte membrane fuel cells (Gostick et al., 2009), water filtration membranes, biomaterials, and many other types of porous media. However, the scope of this review is limited to geological porous media (reservoir rocks and soils). It also discusses the fundamentals of rate-controlled porosimetry and immiscible displacement processes, critical developments in rate-controlled porosimetry, and applying this technique to reservoir characterization and pore-scale modeling of fluid flow in geological porous media.

Fundamentals of Rate-Controlled Porosimetry and Immiscible Displacement Processes

The fluctuations in a rate-controlled capillary pressure trace are termed rheons, risons, and subisons. These terms were developed over approximately six decades as various researchers studied capillary phenomena in porous media. Their origins will be explored in this section.

Rheon/ Haines Jump

A rheon is a spontaneous and irreversible drop in pressure on the drainage capillary pressure trace, indicating the onset of a non-wetting fluid invading a region of low capillarity (pore body) during a drainage process. Melrose (1965) discussed the normalized curvature of the non-wetting meniscus with constant mean curvature as a function of the position of the interface curvature relative to a pore opening and the type of pore opening in an

ideal soil model (defined as consisting of perfect spherical soil grains of identical size). This model demonstrated that decreasing the advancing meniscus curvature would cause instability in the fluid configuration, resulting in an interface jump. The interested reader is referred to Gibbs (1878) for a discussion on the stability conditions of immiscible fluid configurations.

In a five-part study, Haines (1930) performed analyses on an "ideal soil" to study capillary cohesion between soil grains and capillary behavior in the pore space as a function of moisture content. He noticed that the filling and emptying of pore bodies resulted in capillary pressure fluctuations, which he referred to as micro-oscillations. These micro-oscillations were later called jumps by Miller and Miller (1956). Melrose (1970) referred to these jumps as rheons. After that, Morrow (1970) adopted the term to refer to an isovolumetric interface jump. Melrose (1974) further distinguished rheons, which occur during drainage as xerons, and rheons, which occur during imbibition as hygrons. Heller (1968) suggested that Melrose referred to rheons, which occur during drainage as dryons and rheons, which occur during imbibition, as wetons. These distinguishing terms for rheons have yet to be used in recently published literature.

Yuan and Swanson (1989) provided a cursory discussion of the factors that affect the details of the interface jumps in rate-controlled porosimetry measurements. These factors are the rate of injection, shape of the pore bodies being invaded, matrix permeability, snap-off, restrictions on the entry into the core plug, the entry pressure into the pore space, and the core plug's bulk volume used for the measurement.

The shape of a pore body affects the curvature of the non-wetting phase meniscus. As an example, Yuan and Swanson (1989) state that the tubular pore bodies, which are more prominent in the San Andres dolomite than the Berea sandstone, cause smaller rheons. For a spherical pore body, the pressure drop will be more significant than that for a tubular pore body because of the difference in pore aspect ratio (i.e., the ratio of the pore body diameter to the pore throat diameter) between the two pores. The pore aspect ratio will be larger for the spherical pore body if the length of the tubular pore body is equal to the diameter of the spherical pore body and both have equal pore volumes. **Fig. 1** shows spherical and tubular pore body cross-sections connected to a pair of equally sized pore throats.

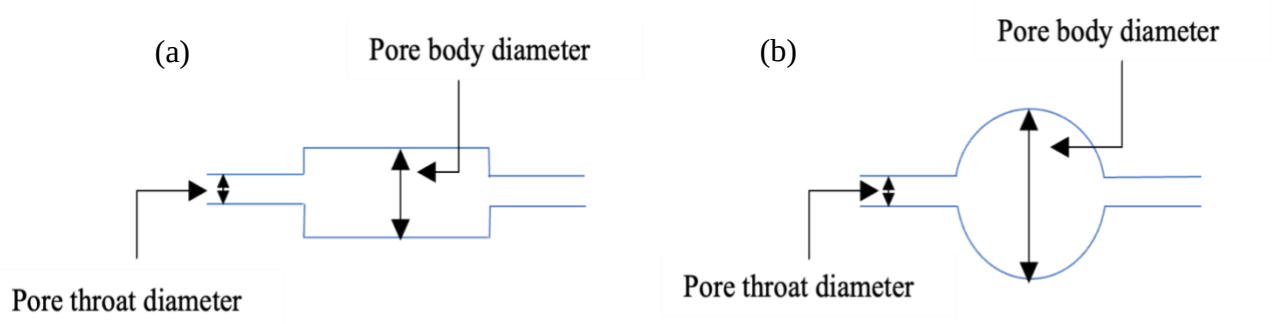

Fig. 1 – Cross-section of a pore body showing a difference in pore aspect ratio for differently shaped pore bodies: (a) Tubular pore body; (b) Spherical pore body.

The pore throat size distribution governs the matrix permeability. Procedures have been developed by Purcell (1949), Swanson (1981), and Thomeer (1983), among others, to empirically relate the capillary pressure curve of a rock sample to its single-phase permeability based on the bundle of tube pore structure model. It is, therefore, vital to understand their measurement in detail.

During an interface jump during drainage, the volume of the non-wetting phase which invades the new pore body is from the non-wetting phase from other saturated pore throats, i.e., the non-wetting phase saturation in the rock sample remains the same (Toledo et al., 1994; Berg et al., 2013). Berg et al. (2013) determined that the flow rate at which the non-wetting phase invades a new pore body at the onset of an interface jump could be one thousand (1000) times greater than the injection rate.

This snap-off occurs when the non-wetting fluid experiences an instability at a pore neck, which causes a portion of the non-wetting fluid to separate from the bulk non-wetting fluid and remain trapped. Yuan and Swanson (1989) state that the capillary pressure can decrease significantly if this occurs near an entry pore system. The magnitude of the snap-off volume is controlled by the pore aspect ratio (Peters, 2012, 129). Yuan and Swanson (1989) suggested this was more likely in the San Andres dolomite, which has a larger pore aspect ratio than the Berea sandstone.

When the non-wetting phase is restricted to entering the pore system of a rock sample from one face instead of all faces, larger interface jumps are realized. Yuan and Swanson (1989) posit that reduced global imbibition results in a larger curvature radius of the meniscus, leading to larger pressure drops as evidenced by a Berea sandstone, which was epoxied on the top and the sides, restricting mercury from entering from the bottom of the rock sample, resulting in larger rheons.

Yuan and Swanson (1989) also report that higher entry pressures result in larger interface jumps. However, this also may be attributed to rock samples with severe pore structure heterogeneity, which consequently results in these rock samples having larger pore aspect ratios.

The bulk volume of a rock sample is related to the surface area of the pore network; hence, the larger the bulk volume, the greater the contributory volume from other pore throats, which results in smaller rheon. Toledo et al. (1994) verified this using Monte-Carlo simulation of low capillary number drainage and imbibition processes in low and high aspect ratio pore network models. This was done to investigate the response of rate-controlled capillary pressure measurements to pore structure to find the optimum sample size for APEX measurements. The low aspect ratio network model required a smaller network size than the high aspect ratio samples to observe pronounced interface jumps. While there were discrepancies between the results obtained for their low aspect ratio sample and the Berea sandstone sample, the results obtained from the high aspect ratio sample were similar to those obtained from the San Andres dolomite sample from Yuan and Swanson (1989). This led to the conclusion that the sample size (0.5-inch diameter by 0.5-inch long core plug) Yuan and Swanson (1989) tested was appropriate.

Ison

An ison indicates a rising pressure level on the capillary pressure trace. It corresponds to quasi-static immiscible displacement in the pore space (Morrow, 1970). On the drainage curve, an ison corresponds to increasing capillary pressure and decreasing wetting phase volume. In contrast, an ison on the imbibition curve corresponds to decreasing pressure and increasing wetting phase volume (Toledo et al., 1994). Isons were subsequently resolved into risons and subisons by Yuan and Swanson (1989). Subisons are the capillary pressure segment between the end of a rheon to the starting pressure level of the rheon, as illustrated in Fig.4 . The volume associated with this segment is used to obtain a pore body size or a pore body system (a group of pore bodies) assuming spherical geometry. Risons are the capillary pressure segment between the end-point of a subison and a higher capillary pressure level before the next rheon occurs, as illustrated in **Fig. 2**. The end-point pressure level of each rison is used to obtain the pore throat size assuming cylindrical geometry using the Washburn (1921b) equation.

Pressure Responses for Rate-controlled Drainage

Rate-controlled drainage is the non-wetting phase immiscibly displacing the wetting phase at a controlled volumetric flow rate. This cooperative pore-filling event involves multiple pore bodies and throats in proximity to a given pore body being filled (Yuan and Swanson, 1989; Toledo et al., 1994; Armstrong and Berg, 2013; Berg et al., 2013, 2014).

Simple pore-filling events for a piston-type drainage mechanism are illustrated to elucidate the inference of pore throat and body sizes from a rate-controlled capillary pressure trace. For in-depth discussions of drainage mechanisms, the reader is referred to Lenormand et al. (1983).

As non-wetting fluid is injected at a low and constant volume flow rate into the rock sample, the meniscus curvature increases; hence, the capillary pressure increases, as shown in Fig. 2. This segment of the capillary pressure curve is known as a rison.

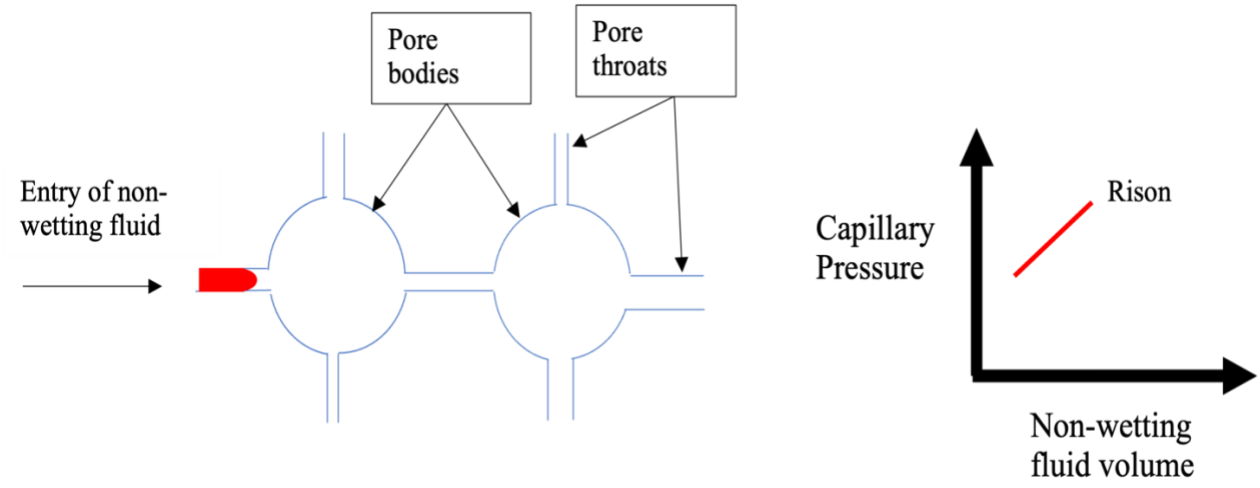

Fig. 2 – A rison in a capillary pressure trace of a drainage process in a simple pore system (Daniels et al. 2023).

The Young-Laplace equation, **Eq. 1**, relates the capillary pressure between two immiscible fluids to the curvature of their interface (Young, 1805; Laplace, 1807).

$$P_c = \sigma\left(\frac{1}{r_1} + \frac{1}{r_2}\right) \quad (1)$$

When the immiscible fluids are in contact with a solid surface, a contact angle, θ, is introduced into Eq.1. In the instance where the geometry of the solid surface is cylindrical, which is normally the assumed geometry for a pore throat, each principal radius, r_1, and r_2 is replaced by $r/\cos\theta$ and Eq. 1 becomes **Eq. 2**. The radius of curvature of the interface between the immiscible fluids, r, is equivalent to the pore throat radius. Therefore, pore throat sizes can be estimated from the end-point pressure level of a rison using Eq. 2. The Young-Laplace equation in this form is often referred to as the Washburn equation (Washburn, 1921b).

$$P_c = \frac{2\sigma|\cos\theta|}{r} \quad (2)$$

As the volume of non-wetting fluid injected into the pore system increases, the capillary pressure eventually becomes greater than the threshold pressure level required to invade the neighboring pore body. The non-wetting fluid meniscus experiences instability; the meniscus curvature decreases rapidly with an accompanying pressure drop. This pressure drop occurs until the curvature reaches a stable configuration, as shown in **Fig. 3**. This rheon is primarily a result of a fluid reconfiguration in which the menisci from the connected phase of the liquid in other pore throats retracts (global imbibition). This cumulative retracted volume is what invades the pore body. The speed at which a pore body is drained depends on the amount of fluid stored in the meniscus of the non-wetting fluid and far exceeds the injection rate from the pump by as much as a thousand (1000) times (Berg et al., 2013). This implies that the rheon occurs at a constant volume. Berg et al. (2014) experimentally observed that interface jumps occurred within 1 to 10 milliseconds. A temporal resolution between 10 to 30 seconds is sufficient to visualize changes in pore-scale displacement events in such experiments (Berg et al., 2013) because interface jumps occur every 10 to 20 seconds (Berg et al., 2014).

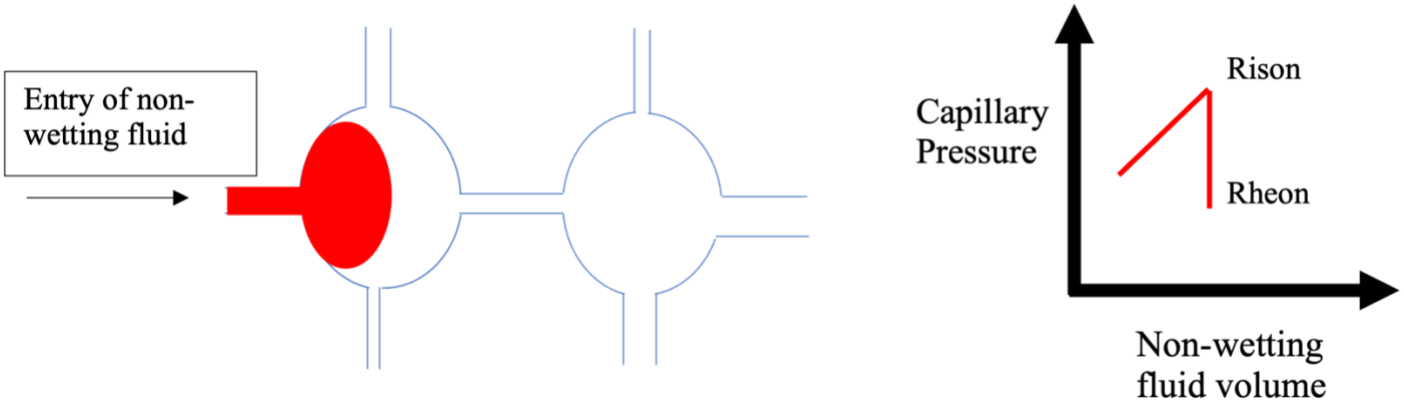

Fig. 3 – A rheon in a capillary pressure trace of a drainage process in a simple pore system (Daniels et al. 2023).

The pore body or group of pore bodies are filled, and the capillary pressure returns to its initial level prior to the rheon. The first rheon is the primary rheon, and a subsequent rheon is referred to as secondary. Pore body sizes are estimated from the subison volume depending on the pore body geometry assumed. The subison volume is the volume of non-wetting fluid in between two risons. For a spherical pore body, **Eq. 3** can be used to obtain to obtain the pore body size.

$$V = \frac{\pi}{6} d^3 \quad (3)$$

The simple case of two subisons in a pore system is illustrated in **Fig. 5**. When a secondary rheon is present, Mason (1991) states that the volume of the subison associated with the primary rheon should be computed by extending the pressure gradient of the subison to intersect the threshold pressure indicated by the dotted line. The volume difference between this intersection and the initial volume point of the primary rheon is the volume of the

primary subison. In contrast, the volume associated with the second subison is the volume difference between the end-point of the subison and the intersection point of the first subison and the threshold pressure level. Yuan (1991a) agrees with Mason (1991) that, a failure to compute the individual subison volumes in this manner would result in overestimating the pore volume associated with the first subison and underestimating the volume associated with the second subison.

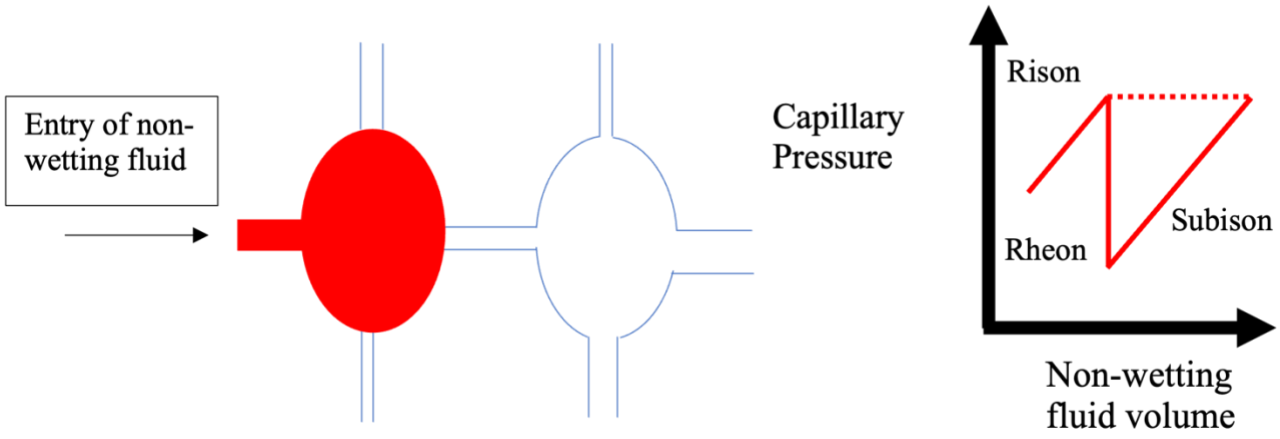

Fig. 4 – A subison in a capillary pressure trace of a drainage process in a simple pore system (Daniels et al. 2023).

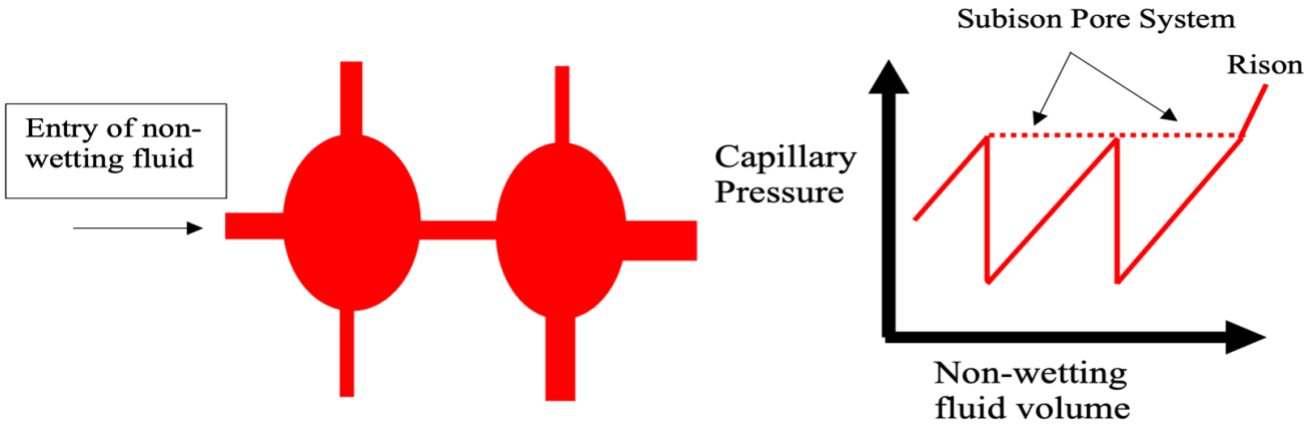

Fig. 5 – A subison pore system in a capillary pressure trace of a drainage process in a simple pore system (Daniels et al. 2023).

Pressure Responses for Rate-controlled Imbibition

Imbibition is a wetting phase immiscibly displacing a non-wetting phase at a controlled volumetric flow rate. Few rate-controlled displacement imbibition studies, such as Berg et al., 2014 and Singh et al., 2017 have been performed in rock samples.

Simple pore-filling events for imbibition (**Fig. 6** through **Fig. 8**) are illustrated. The reader is referred to Lenormand et al. (1983) and Toledo et al. (1994) for in-depth discussions of imbibition displacement processes. These studies were not performed in geological porous media.

As wetting fluid displaces non-wetting fluid, the non-wetting fluid's meniscus curvature decreases; hence, the capillary pressure decreases, as shown in Fig. 6. This segment of the capillary pressure curve is a rison.

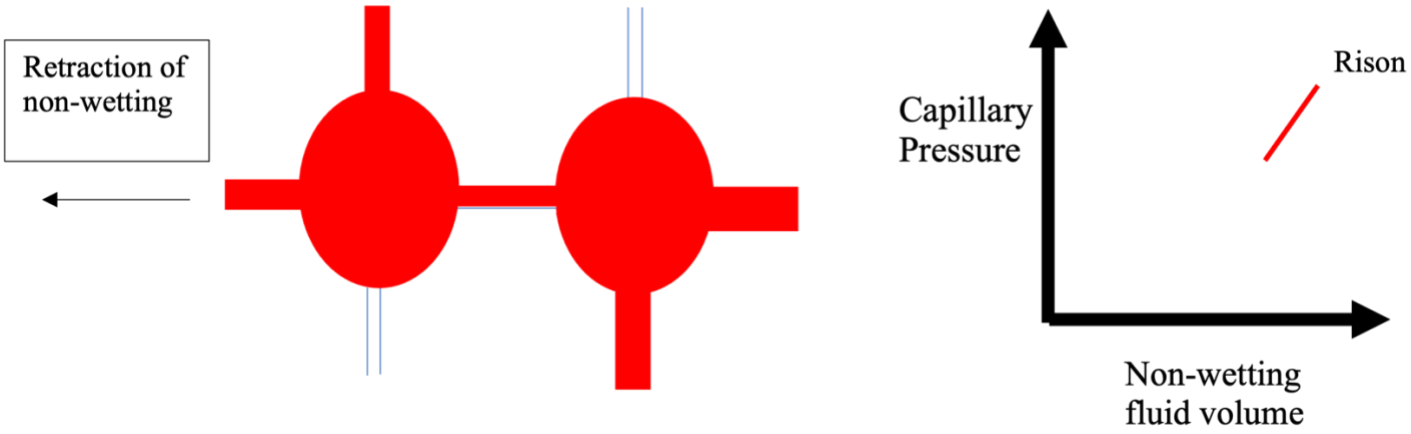

Fig. 6 – A rison in a capillary pressure trace of an imbibition process in a simple pore system.

As the process continues, the non-wetting phase 'snaps off' and becomes disconnected from the bulk non-wetting fluid. Singh et al. (2017) found that a snap-off event typically takes 10 minutes to complete, a process which is approximately five orders of magnitude slower than interface jumps, which occur in 1 to 10 milliseconds during drainage, according to Berg et al. (2014). Snap-off leads to capillary trapping. At this point, the capillary pressure increases until the non-wetting fluid reaches a stable configuration.

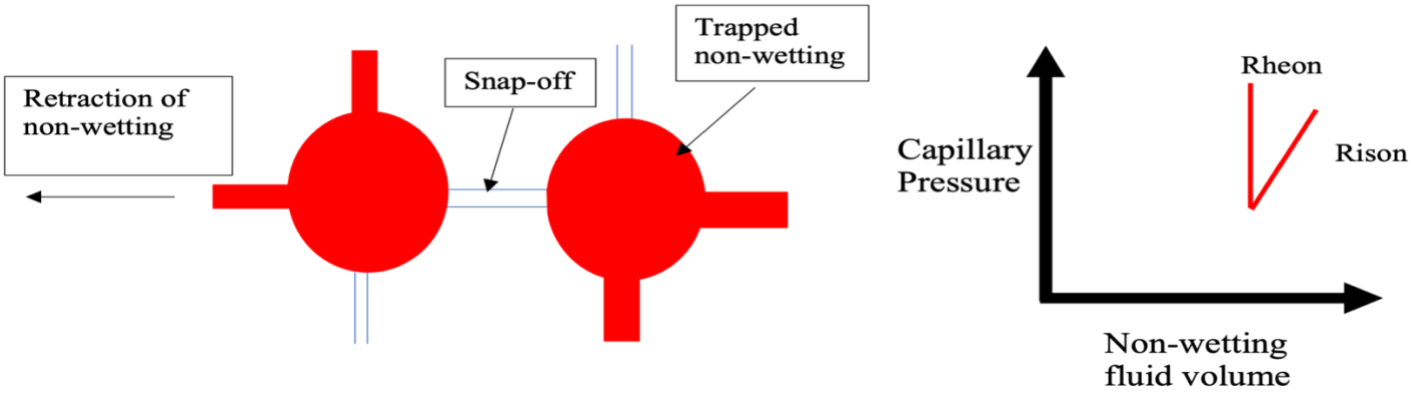

Fig. 7 – A rheon in a capillary pressure trace of an imbibition process in a simple pore system.

The non-wetting fluid is finally displaced from the entire pore body or group of pore bodies, and the capillary pressure decreases to the pressure level of the preceding rheon. The capillary-trapped non-wetting fluid is responsible for the residual saturation. Yuan and Swanson (1989) assumed the residual saturation from an APEX measurement is equivalent to the total subison volume and validated this assumption via residual/initial curves from a countercurrent imbibition measurement.

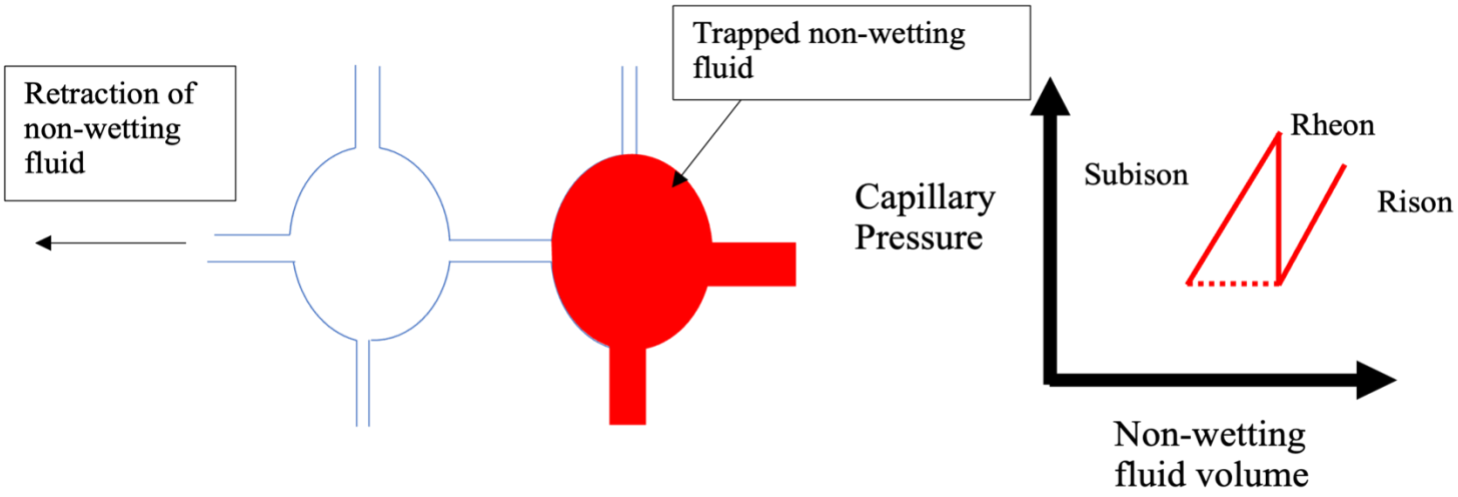

Fig. 8 – A subison in a capillary pressure trace of an imbibition process in a simple pore system.

Developments in Rate-Controlled Porosimetry Instrumentation and Techniques

All rate-controlled porosimetry instrumentation systems share key instrument components. These are a hydraulic piston pump that controls the injection and withdrawal rates of the non-wetting phase, a sample chamber that contains the rock sample being tested, a reservoir that contains the non-wetting fluid to be injected, temperature control of keeps the temperature of the sample chamber, since the thermodynamic properties of the non-wetting fluid (i.e. contact angle and interfacial tension) are sensitive to temperature and a data acquisition and control system which is used to control the various instruments, as well as record and store the necessary data, such as pressure and volume of non-wetting fluid injected.

Rate-controlled porosimetry instrumentation and techniques have been introduced by different names in various disciplines. The following are some of the unique names assigned to this technique: Apparatus for Pore Examination (APEX) by Yuan and Swanson (1989), volume-controlled porosimetry by Toledo et al. (1994), time-controlled porosimetry by Cerepi et al. (2000), Constant Rate Air Injection (CRAI) by Chatzis and Rezaei (2006), Capillary Pressure Spectrometry (CPS) by Sygouni et al. (2006) which refers to their analyses of the resultant capillary pressure trace using wavelet analysis and lastly fast X-ray micro-CT (a synchrotron micro-CT scanner with an in-built APEX) by Berg et al. (2013). The timeline below shows key developments in rate-controlled porosimetry instruments and techniques.

1966

Crawford and Hoover design and construct a rate-controlled porosimetry instrument with a volumetric resolution of 10^{-5} cm^3 to characterize pores in terms of volume and infer pore shapes from the data obtained.

Morrow perform rate-controlled porosimetry measurements to study the mechanisms and thermodynamics of rate-controlled immiscible displacement processes.

1970

1971

Gaulier design and construct a rate-controlled porosimetry instrument to characterize vuggy porosity. The instrument has a volumetric accuracy of 1 mm^3 per stroke.

Yuan and Swanson introduce the Apparatus for Pore Examination (APEX) and the data is used to resolve the pore space into pore throats and bodies. The instrument has a pressure resolution of 0.002 psi and volumetric resolution of 10^{-7} cm^3.

1989

1991

Yuan (1991a) uses APEX data to determine cementation exponent (m) and absolute permeability. Yuan (1991b) uses APEX data to measure pore-scale heterogeneity and the effect of pore geometry on the efficiency of a waterflood program.

Toledo et al. run a rate-controlled porosimetry computer simulation in a pore network model to study APEX responses.

1994

1998

Knackstedt et al. run a rate-controlled mercury porosimetry computer simulation on a correlated grid to show the need to account for correlation in pore-scale heterogeneity in invasion percolation models.

Cerepi et al. introduce time-controlled porosimetry to determine the complexity of the pore space of a calcareous material.

2000

2001

Knackstedt et al. extend the work done in 1998 to simulation of two-phase flow in pore network models.

Cerepi et al. use time-controlled porosimetry to analyze the pore-scale dynamics of capillary flow and use the data to compute single and multiphase transport properties of calcareous rocks with different textures.

Chen and Song integrate the results of constant rate mercury injection, NMR and thin sections to accurately determine pore body size distributions and the shape of the pore bodies in a Berea Sandstone sample.

2002

2005

Smith et al. introduce constant rate air injection to determine breakthrough capillary pressure in a brine-saturated Berea core plug sample and water-saturated glass micromodels.

2006

Sygouni et al. introduce the use of wavelets to decompose the rate-controlled capillary pressure data and correlate the amplitude peaks to the spatial distribution of fractional wettability.

2009

Aggelopoulos and Tsakiroglou develop a multi-flowpath (MFPM) model to quantify heterogeneities at the microscopic and macroscopic length scales.

2011

Rezaei and Chatzis use constant rate air injection to characterize vugs in porous media.

2012

Constant rate mercury injection is combined with low-field NMR spectral analysis and micro-CT imaging to characterize the pore size distribution of vugs.

2013

Berg et al. use the Fast synchrotron-based micro-CT with sub-second temporal resolution to image Haines jumps and immiscible displacement events.

2014

Armstrong et al. (2014a) validate a macroscale definition of capillary number from Hilfer and Øren (1996) using fast X-ray micro-CT to show that non-wetting phase mobilization occurs at a macroscopic Capillary Number of approximately 1 instead of the conventional microscopic Capillary Number of 10^{-5}

Armstrong et al. (2014b), introduce an approach to study multiphase flow under dynamic capillary flow conditions at the pore-scale using the fast micro-CT. In this method, 2D radiographs are analyzed to reconstruct a 3D image of the highest quality possible to study displacement processes which occur on a timescale of 40 milliseconds.

2017

Singh et al. use fast synchrotron X-ray micro-CT to provide insights into pore-filling imbibition events and snap-off.

Moura et al. observe $1/f^{\alpha}$ power spectra associated with rate-controlled events in porous

2020

Bultreys et al use fast synchrotron X-ray micro-CT to validate the capability of pore network models to predict fluid distribution.

2022

Gostick et al. (2022) developed an algorithm to simulate rate-controlled displacement on images which produced better phase trapping results compared to that of pressure-controlled displacement.

Application to Reservoir Characterization

Reservoir Characterization involves analyzing a reservoir to determine its properties to build a representative model that can be used to predict reservoir behavior and performance. Detailed and accurate reservoir characterization will improve hydrocarbon recovery, site selection for geological carbon storage, and geothermal energy exploitation. Capillary pressure data allows for estimating petrophysical properties such as porosity, absolute and relative permeability, residual hydrocarbon saturation, initial fluid saturation, and distribution in the reservoir and pore structure. This section will explore applying rate-controlled porosimetry techniques to estimate these properties.

Pore Structure Characterization

Pore structure characterization is important in the hydrocarbon exploration and production phase of field development to assess and understand reservoir rock's storage capacity (porosity), fluid distribution, and hydraulic conductivity (absolute permeability). Rate-controlled porosimetry allows pore structure information (pore body and throat size distributions, pore shape, pore surface roughness) to be compared with pressure-controlled porosimetry, MICP, which provides only pore throat size distributions, Nuclear Magnetic Resonance (NMR) and Gas Sorption, both of which are best suited to provide pore body size distributions. These experimental and imaging techniques are employed in an integrated approach to characterize the pore structure of various conventional and unconventional rock samples.

History of Pore Body and Throat Size Distribution Measurements

Yuan and Swanson (1989) pioneered using rate-controlled porosimetry, APEX, to obtain rock samples' pore body and throat volume distributions. The technique was tested on twin samples of Berea sandstone and San Andres dolomite core plugs. Due to the limited volumetric resolution of their measurement system (10^{-6} cc), it was only possible to resolve mesopores (62 μm – 4 mm) but not possible to resolve micropores (< 62 μm) according to the classification of Choquette and Pray (1970). Recent APEX studies on the Berea sandstone, comparing results obtained from petrographic analyses in literature, confirm that most subisons/subison pore systems fall within the mesopore range (Mahmud, 1998; 2022). Yuan and Swanson (1989) developed a classification scheme for subison pore systems, partitioning them into thirteen (13) class sizes of increasing volume ranges as shown in **Table 1**. The pore space information was presented in two ways. The first method was to show subisons pore system distribution over various pressure ranges. In contrast, the second method showed incremental fractional volume as a function of either saturation (within a 5% saturation range) or pressure (within two (2) psi pressure range).

Table 1 – APEX Volume Classification Scheme by Yuan and Swanson (1989)

Class Size	Volume Range (nL)
4	0.69 – 1.47
5	1.48 – 3.03
6	3.04 – 6.16
7	6.17 – 12.4
8	12.5 – 24.9
9	25.0 – 49.9
10	50.0 – 99.9
11	100 – 199.0

12	200.0 – 399.0
13	400.0 – 799.0
14	800.0 – 1599.0
15	1600.0– 3199.0
16	≥ 3200.0

APEX has also been applied to rock cuttings, which are usually widely available and inexpensive compared to core samples, to extract porosity and permeability reliably (Siddiqui et al., 2005). This study combined APEX with NMR to obtain pore and throat size distributions from the cuttings of an Arab-D rock sample. While the pore size distribution results obtained from both techniques were in agreement, for pore throat size distribution, APEX showed a multimodal distribution, which NMR did not. This illustrates the limitations of NMR to reveal pore throats.

In recent years, rate-controlled porosimetry has been used in combination with other experimental and imaging techniques to assess pore size distributions in coals accurately (Yao et al., 2012), in Bentonite (Liu et al., 2020) to assess the sealing ability for underground nuclear waste disposal. Rock samples from tight dolomite (Xie and Guan, 2019), tight sandy conglomerate (Chen et al., 2018), and a multitude of tight sandstone reservoirs located in some of the most productive basins in China such as the Ordos Basin (Zhao et al., 2015a; Zhao et al., 2015b; Zhao et al., 2015c; Gao, 2016; Wu et al., 2018b; Wang and Zeng, 2020; Meng et al., 2021), Songliao Basin (Xiao et al., 2016a; Xiao et al., 2016b; Xi et al., 2016), Sichuan Basin (Zhao et al., 2018; Zhang et al., 2020) and Y Basin (Zhao et al., 2019) were also measured.

The advent of hydraulic fracturing and horizontal well drilling technology has enabled the production of hydrocarbons from unconventional and tight reservoirs in commercial quantities, though their ultimate recovery remains low. This has attracted much research interest and activity to understand and better assess their physical properties to optimize recovery. In most of these studies, the rate-controlled porosimetry instrument of choice was the ASPE – 730 Automated System for Pore Examination following the standard Q/SY DQ 1531-2012 of Daqing oilfield in China. Mercury was injected at 5E-5 ml/min (8.33E-7 cc/s), equivalent to a pore body diameter of 117 microns filled every second, assuming spherical geometry. The maximum pressure applicable is 6.2 MPa (~900 psi), equivalent to a pore throat size of 0.12 um, assuming cylindrical geometry.

Effects of Pore Shape

A priori knowledge of pore geometry is necessary to obtain a pore size distribution from a capillary pressure trace. Historically, spherical geometry has been assumed for pore bodies, while cylindrical geometry has been assumed for pore throats based on sphere packing (Slichter, 1899; Kozeny, 1927; Carman, 1937; Brooks and Purcell, 1952) and bundle of capillary tube models (Purcell, 1949; Childs and Collis-George,1950; Fatt and Dykstra, 1951; Burdine, 1953) respectively. These geometrical assumptions result in simple boundary conditions to solve the Young-Laplace equation. This is a nonlinear partial differential equation in its original form. However, these geometrical assumptions may not represent the actual pores of a reservoir rock, resulting in an overestimation of pore sizes. The wetted pore surface area-to-volume ratio is inversely related to absolute permeability and is a function of the pore shape and size. A spherical pore body has the smallest surface area-to-volume ratio of any pore shape and provides the highest porosity and permeability, all other parameters being equal. Therefore, a failure to account for a representative pore shape results in overestimating the petrophysical properties. Chen and Song (2002) integrated the analyses of rate-controlled porosimetry and NMR measurements of Berea sandstone to conclude that the shape of pores in the Berea was tube-like oblong and spherical pore geometry assumptions resulted in overestimated pore body sizes. This conclusion was supported by thin section analysis.

Rate-controlled porosimetry has also been used exclusively to provide information on pore body shape due to its effect on a rheonic pressure response. The slope of a rheon is related to the pore aspect ratio, which can be used to infer the shape of a pore body. Crawford and Hoover (1966) studied multiphase flow (air-water) in energy terms. Cylindrical Pyrex tubes with glass beads of different packings were used as the porous media. The diameter of the glass beads differed between each tube but were equal within the same tube. The tubes with greater packing had smaller diameter glass beads, and the pore shapes varied with the packing of the glass beads in each tube. The area under this differential pressure versus volume injected curve was equated to work done by the pump on the system, assuming the water is incompressible. The volume of a pore was defined as the volume between two successive rheons. The authors plotted work per pore against pore volume and observed a linear relationship with the constant of proportionality specific to a type of packing, provided the shapes of the pores in a given tube are the same. This linear relationship showed that surface area increased linearly with pore volume, provided pore shapes were similar. However, when the pore shapes differed, the specific surface area of the pore changed along with the constant of proportionality between work per pore and pore volume.

Effects of Pore Structure Heterogeneity

Due to the effects of deposition and diagenesis on grain size and texture, pore structure heterogeneity is typically present at multiple length scales in naturally occurring porous media. Accounting for heterogeneity is important to assess and model petrophysical properties, predict reservoir performance, and optimize secondary/tertiary hydrocarbon recovery programs.

Carbonate rocks usually have relatively complex pore systems due to the more pronounced effects of diagenetic processes (i.e., chemical and biological) they undergo. Pore types contributing significantly to heterogeneity include vugs, interparticle porosity, and microporosity. Vugs are considered macroscopic heterogeneities and, as a rule of thumb, are defined as a pore larger than three times the median grain size. Myers (1991) defines microporosity as the pores too small to be seen on a thin section under 10x magnification. Swanson (1985) defines microporosity as pores significantly smaller than those contributing to the rock's permeability. These individual pore systems can be studied using rate-controlled porosimetry. Gaulier (1971) built a rate-controlled porosimetry device to measure vuggy porosity in heterogeneous rock samples to facilitate the assessment of secondary recovery methods. This device had a pressure range of 10000 psi and volume displacement resolution of 1 mm^3 per stroke, and each four-switch pressure transducer had an accuracy of 0.5% of its measuring range. In a similar context, Chatzis and Rezaei (2006) developed a Constant Rate Air Injection (CRAI) apparatus that injects air at a constant rate into a sample filled with wetting phase (water) to characterize vugs of volume $1mm^3$ and larger. This apparatus was tested on packs of sintered glass beads with artificially created vugs. The measurements obtained agreed with the vug sizes created. Rezaei and Chatzis (2011) further investigated mechanisms of pore-scale drainage and the effect heterogeneities have on the response of their CRAI apparatus.

Pore-scale heterogeneity has been characterized using multiple techniques. Yuan (1991a) developed the Final Oil Saturation Model (FOSMOD) factor, using APEX data to assess pore-scale heterogeneity quantitatively. The FOSMOD factor, which ranges from 0 to 1, was defined as the ratio of oil volume recovered from a given subison pore system to the volume of the associated subison pore system. A FOSMOD factor of 1 represents maximum homogeneity, while a factor of 0 represents the maximum heterogeneity. The application of FOSMOD to strictly assess the efficiency of secondary recovery methods will be discussed later. Cerepi et al. (2000) introduced time-controlled mercury porosimetry (a misnomer due to the similarity in experimental set-up to other rate-controlled porosimetry instruments) where separate plots of mercury volume versus time and capillary pressure versus time are analyzed to establish two sets of parameters based on the numerical derivative of the capillary pressure curve (penetration thresholds) and time for mercury to fill the pore space to describe heterogeneity at the pore-scale.

Thompson et al. (1987, 630-644) presented various studies which show the fractal nature of geological porous media from imaging analysis using correlation measurements, chord-length measurements among others. The power or amplitude spectra of rate-controlled capillary pressure curves of geological porous media are "$1/f^{\alpha}$" signals (Spurin et al., 2022; Daniels et al., 2023). This indicates their self-affine fractal properties. The fractal dimension has been used to quantify pore-scale heterogeneities by comparing pore size distributions obtained from pressure controlled along with rate-controlled porosimetry (Wang et al., 2018; Dazhong et al., 2019; Lin et al., 2021). Daniels et al. (2023) estimated the fractal dimension as a spatially correlated pore structure heterogeneity index from high resolution rate-controlled capillary pressure curves for a sandstone and carbonate core plug. The degree of heterogeneity was proportional to the fractal dimension, which ranges between 2 and 3. Aggelopoulos and Tsakiroglou (2009) developed the multi-flowpath model (MFPM) to quantify heterogeneities at the microscopic and macroscopic length scales. The MFPM characterizes the pore space of a soil column as a system of parallel paths with varying permeabilities. Each flow path's permeability represents an average over a particular pore length scale, and the variability in permeability between flow paths represents the macro heterogeneity of the soil column. These properties and other coefficients are obtained from the pressure response of a rate-controlled drainage process. It was found that the capillary pressure curves from this model are consistent with MICP results over a low-pressure range and irreducible water saturation, and its associated end relative permeability increases with increasing soil heterogeneity.

Fractured reservoirs exhibit a high degree of heterogeneity, which significantly impacts fluid flow because fractures (megascopic heterogeneities) create additional pathways for fluid flow within a reservoir, which causes an uneven distribution of flow. Tsang and Hale (1988) related the concepts of resolving the pore space statistics using rate-controlled porosimetry from Yuan and Swanson to investigate fracture aperture parameters controlling fluid flow and tracer transport in fractures. Two fractures were mathematically modeled as planes filled with varying aperture sizes with lognormal density distribution and spatial correlation lengths. Their mercury simulation showed the rison curve could be used to obtain information on the small aperture sizes that control flow permeability in a single fracture. These small apertures were posited to control the flow permeability because they can act as flow barriers to larger-sized apertures until they are filled. This is akin to the role of pore throats acting as flow constrictions to pore bodies until they are filled. Moreover, simulated pressure-controlled porosimetry provided information on the size distribution of apertures, which control tracer transport. Withdrawal experiments were simulated, and an inverse relationship between trapped mercury and spatial correlation length was found.

Prediction of Transport and Fluid Properties

Pressure-controlled capillary pressure data is routinely used to estimate permeability (Swanson, 1981; Thomeer, 1983; Katz and Thompson, 1986). Since rate-controlled capillary pressure data provides information about the pore throats and the pore bodies that interconnect them, improved permeability models can be inferred from them, particularly in carbonates where vugs are important (Myers, 1991). Yuan (1991b) developed rison and subison bivariate distribution functions, characterized by entry pressure and volumes, to express pertinent petrophysical properties such as absolute permeability and cementation exponent, residual non-wetting phase saturation, as a function of pore-scale attributes. Cerepi et al. (2002) use time-controlled porosimetry to develop expressions from an extended Washburn (1921b) equation by Sorbie et al. (1995), accounting for pore filling time as a function of pore aspect ratio to estimate absolute permeability effective and relative permeability during a drainage process. The authors validated their results with absolute permeability measurements from 30 samples of Oligocene carbonate rocks from the Aquitaine basin and established a good correlation between the measured and calculated absolute permeability. They also found that effective relative permeability depends on texture and pore structure. Smith et al. (2005) developed an experimental technique, constant rate air injection (CRAI), to determine breakthrough capillary pressure related to a porous medium's absolute permeability. Breakthrough capillary

pressure is the pressure at which a non-wetting phase can flow through a porous medium from an entry to an outlet face. However, the breakthrough capillary pressure, as defined by Smith et al. (2005), can only be considered equal to the entry capillary pressure for porous media with narrow pore size distributions (i.e., homogenous porous media). Water-air displacement tests were performed in two micromodels, one of which was made of glass beads sintered between glass plates, and the other which was a micromodel made of capillary networks etched on glass plates. Both micromodels were initially filled with water. The rock sample was a brine-saturated Berea sandstone core plug epoxied on its sides to restrict entry and exit of fluids to the two faces across its length. Videos of the tests were recorded, and the tests were validated with capillary drainage height tests. The breakthrough capillary pressure was determined as the highest pressure recorded before the breakthrough of the invading fluid occurred and was shown to have an inverse relationship with permeability for the micromodels. The breakthrough capillary pressure results determined using power-law models to determine permeability agreed with experimental results. The breakthrough capillary pressure and permeability power law models used had similar exponents to the power law model for permeability and breakthrough capillary pressure for the micromodels, which the authors suggest could be a medium-independent relationship between breakthrough pressure and permeability. This suggestion and the conclusions of Moura et al. (2017) disagree with Thompson et al. (1987a) on micromodels' usefulness in relating rock properties to pore structure. While the working principle of constant rate air injection is similar to other rate-controlled porosimetry techniques, using air as the non-wetting phase is unsuitable for obtaining detailed pore geometry information.

Capillary pressure plays an essential role in hydrocarbon recovery. Yuan (1991a) used his final oil saturation model (FOSMOD) to determine the final residual oil saturation (S_{of}) after a tertiary (Enhanced Oil Recovery) or secondary recovery mechanism (waterflooding). The residual oil saturation (S_{or}) from primary recovery is obtained by normalizing the sum of subisons pore system volume to the pore volume of the rock sample based on the assumption that all the oil in subisons pore systems is trapped (Yuan and Swanson, 1989). The final oil saturation is a function of the recoverable oil from a subison pore system (E_{Ri}), as shown in **Eq. 4**. This implicitly makes it a function of the pore-scale heterogeneity (FOSMOD factor) discussed earlier.

$$S_{of} = \sum_{i=1}^{N_s} \frac{V_{si} - E_{Ri}}{V_p} \tag{4}$$

The final oil saturation and residual oil saturation (considered as the ratio of subison volume to total pore volume) computed from APEX data can be used to quantify the macroscopic heterogeneity of a reservoir rock through a volume averaged FOSMOD factor as shown in **Eq. 5**. The volume averaged FOSMOD factor has also been used to describe EOR displacement efficiency.

$$\bar{F}_{fV} = \frac{S_{or} - S_{of}}{S_{or}} \tag{5}$$

Influence of Wettability

Wettability is primarily influenced by the rock's mineralogy, surface chemistry, and saturation history and plays a significant role in the fluid distribution, capillary pressure, and transport properties. Therefore, capillary pressure curves generated using wetting fluids can be used to infer the wettability of a porous medium.

Sygouni et al. (2006) developed capillary pressure spectrometry, which uses a bi-orthogonal wavelet function to decompose and analyze the fluctuations of a rate-controlled capillary pressure trace generated by deionized water colored with methylene blue displacing silicon oil (imbibition) in a fractionally wet micromodel (intermediate-wet glass spheres mixed with strongly oil-wet Polytetrafluoroethylene (PTFE) spheres). The decomposed rate-controlled capillary pressure trace, a spectrum of amplitude peaks, is called a capillary pressure spectrum due to its resemblance to the response from spectroscopic analyses. The pressure drop across the porous medium is recorded for twenty (20) seconds, and in a similar time interval, the displacement process is also imaged. The peaks in the capillary pressure spectrum were used to identify the specific mesoscopic flow events in the images, which are classified into either the motion in pore clusters, capillary fingering, or coalescence of interface categories. The peaks of the capillary pressure spectrum are then correlated with the spatial distribution of fractional wettability in the porous medium characterized by a statistical distribution of local coefficients of wettability (F) in associated images where the porous medium has been invaded by water.

Application to Pore-Scale Modeling of Single and Multiphase Fluid Flow

Pore-scale modeling is important for studying and predicting subsurface porous media's single and multiphase flow and transport properties. It is increasingly used to complement core analysis to reduce the uncertainty of assessing reservoir properties. These petrophysical rock properties at continuum scales are governed by pore-scale attributes (Swanson, 1985; Myers, 1991; Yuan, 1991b) and play an important role in the geological storage of CO_2 (Bachu, 2008), primary, secondary, and tertiary recovery of hydrocarbons and the safe disposal of nuclear waste underground.

Representative pore-scale models should include pore structure (pore body and throat size distributions and connectivity) characterized at multiple length scales (Bryant and Blunt, 1992; Bryant et al., 1993; Coles et al., 1996; Balcewiz et al., 2021). These are multiscale pore models and consist of pore network and direct pore-scale models. Pore network models represent the pore space with a network of simplified pore geometries; a thin cylinder represents a pore throat, while a sphere represents a pore body (Chandler et al., 1982; Koplik, 1982). Direct pore-scale models simulate fluid flow on an image of the pore space obtained from an imaging modality. Incorporating the appropriate level of pore structure detail (heterogeneity) to construct geologically representative multiscale pore models with satisfactory predictive accuracy has been challenging in pore-scale modeling and remains a research topic. Improvements have been made in the past two decades (Celia et al., 1995; Øren et al., 1998; Lerdahl et al., 2000; Blunt, 2001; Meakin and Tartakovsky, 2009; Masalmeh 2015; Golpavar et al., 2018; Ruspini et al., 2021). Rate-controlled porosimetry has aided in overcoming the challenges associated with this issue.

Bultreys et al. (2020) use a fast X-ray micro-CT to investigate whether quasi-static pore network models (PNMs), which only consider capillary forces and ignore viscous and inertial forces, can adequately describe fluid configurations at the pore scale while accurately predicting macroscopic scale properties. PNMs represent the pore space with simplified geometric models. The authors came to a positive conclusion at low capillary number flow in strongly water-wet samples with homogenous pore structures. They confirmed that the accuracy of pore geometry description, advancing contact angles volume, and assigning fluid flow conductivity to the pores and throat in the PNM belies the predictive capability of quasi-static PNMs. For more general conclusions on the predictive capabilities of quasi-static PNMs, their validation workflow would have to be applied to multiscale PNMs and complex rocks.

Knackstedt et al. (1998) simulated rate-controlled drainage with a modified invasion percolation algorithm on uncorrelated and correlated lattices (made up of sites and bonds) to investigate if correlation of petrophysical properties existed at the pore scale. The simulation of invasion percolation is similar to rate-controlled immiscible

displacement (Gostick, 2016). The correlated lattices were constructed using fractional Brownian motion (fBm) and had a length scale cutoff of 10 pore sizes in a Berea Sandstone, corroborated by Swanson (1979). It is common practice to validate pore-scale models using capillary pressure and relative permeability curves for single-phase and multiphase flow. The authors found that the capillary pressure curves, especially at higher intrusion saturations, from correlated lattices were representative of experimental capillary pressure curves of the Berea sandstone. In contrast, the capillary pressure curves from uncorrelated lattices were non-representative. Therefore, correlated heterogeneity persists at the pore scale in Berea sandstone, and more importantly, network models used to simulate core-scale processes for a rock sample such as the Berea sandstone (considered homogeneous) need to incorporate correlated heterogeneities to ensure accurate predictions. Knackstedt et al. (2001) furthered this work for two-phase flow in correlated lattices. They observed that predictions were consistent with experimental observations of breakthrough and residual saturations cluster size of trapped non-wetting phase. One of the mechanisms for safely storing CO_2 in geological porous media such as saline aquifers and depleted oil reservoirs is capillary trapping, which is responsible for residual fluid saturation. Therefore, through rate-controlled porosimetry, representative computational rock models with improved prediction of residual fluid saturation can be developed to aid in optimally selecting storage sites for CO_2.

Gostick et al. (2022) developed an algorithm (image-based invasion percolation) to simulate rate-controlled displacement on images and produced better phase trapping results than pressure-controlled displacement. This was possible due to the smaller incremental saturation change from rate-controlled immiscible displacement as opposed to the larger incremental saturation changes from pressure-controlled displacement. Regarding computational efficiency, the results were obtained in 19 seconds compared to 45 minutes for the traditional Lattice Boltzmann method. However, multiphase fluid flow configuration results on a 500 x 500 pixels image from this method were compared to Lattice Boltzmann results with reasonable agreement.

Singh et al. (2018a) collected 496 tomographic images for a complete drainage process (Singh, 2018b) and 416 tomographic images for a complete imbibition process (Singh, 2018c) using a time-series synchrotron X-ray micro-CT with a time resolution of 38 seconds and a voxel resolution of 3.28 μm. Singh (2017) also provides a dataset with residual oil at the end of the imbibition process. These datasets can be found online to validate pore-scale models in other studies, improving segmentation algorithms with limited projections and quantitatively assessing how viscous and capillary forces control non-wetting phase trapping during imbibition.

Discussion and Conclusions

Rate-controlled porosimetry is an effective technique for studying porous media. The increasing pressure and volume resolution of the experimental apparatus due to technological progress in analog-to-digital conversion has progressively made it possible to obtain more information on the properties of porous media using this technique. Yuan and Swanson (1989) leveraged this technological progression to design and construct APEX to obtain pore body and throat size distributions to the mesopore size range. This was previously not possible due to the low resolution of the instruments. Further improvements have increased this to the micropore size range (Berg et al., 2013; Daniels et al., 2023). With greater detail in pore body and throat size distributions, insights into immiscible displacement processes and estimating petrophysical properties such as absolute and relative permeability, cementation exponent in Archie's equation, and residual oil saturation were made possible in conventional reservoirs. Advancements in this technique will continue to provide greater insights into the influence of pore structure and microscopic immiscible displacement on continuum-scale petrophysical properties of geological porous media.

While rate-controlled porosimetry has been effective for pore structure characterization, there remain some challenges with interpreting the measurements. A priori assumptions of the pore geometry must be made to infer

pore body and throat size distributions from the capillary pressure data. Chen and Song (2002) showed that such assumptions could lead to erroneous results if the assumed pore geometry does not represent the actual pore geometry. Therefore, the analyses of rate-controlled porosimetry still need to be combined with other pore structure characterization techniques for validation.

Thus far, imaging modalities have been combined with rate-controlled porosimetry to study multiphase flow and immiscible displacement processes. This has allowed the redefinition of the capillary number at the macroscopic scale to improve the prediction of non-wetting fluid mobilization (Armstrong et al., 2013). Combining imaging modalities with rate-controlled porosimetry allows for improving pore structure characterization of geological porous media. Segmenting the pore space in micro-CT rock images can be anchored with pore space statistics from rate-controlled porosimetry obtained at a similar temporal and spatial resolution. This provides a higher level of objectivity to an otherwise subjective process. In addition to studying immiscible displacement processes, the rate-controlled capillary pressure trace from the fast X-ray micro-CT technique could be matched with the immiscible displacement images for pore structure characterization. Also, this will reduce the uncertainty of differentiating between pore throats and bodies to anchor the segmentation of the pore space of rock images. The acquisition and analysis of micro-CT images can be cost-prohibitive, limiting its use. Acquiring thin sections and digitizing them for petrographic analysis is affordable and could be used as an alternative with rate-controlled porosimetry for pore structure characterization and building digital rock models.

Thus far, rate-controlled porosimetry has offered static descriptions of rock properties. The pore structure of reservoir rocks is dynamic under reservoir conditions during depletion (i.e., change in pore structure as a function of reservoir pressure). As such, future studies can design a rate-controlled porosimeter that accommodates the application of a confining pressure to observe dynamic pore structure characteristics. Improved pore structure characterization will produce computational rock models with enhanced predictive capabilities.

This review introduces the state-of-the-art in rate-controlled porosimetry and the key developments that have led to the current understanding for which this technique is applied in characterizing and modeling geological porous media. Future directions for research using rate-controlled porosimetry techniques were briefly discussed. In summary, rate-controlled porosimetry has been an effective technique for pore structure characterization. It has provided insights into the effect of pore structure on the petrophysical properties of geological and aided in improving the representativeness of computational rock models. Improved quantitative models of geological porous media will result in an improvement of hydrocarbon recovery, site selection for geological CO_2 storage, development and management of geothermal energy sources, and assessment of the sealing ability of engineered barrier systems (e.g. bentonite buffers) for safe underground nuclear waste disposal, all of which are pertinent in addressing global challenges associated with aspects of the energy trilemma (affordability, security, and sustainability).

Nomenclature

α = scaling exponent

θ = contact angle

σ = interfacial tension between non-wetting and wetting fluid, M/T^2

d = diameter, L

f = frequency, Hz, 1/T

r = principal radius, L

E_{Ri} = recoverable oil from the *i*th subison pore system

$\bar{F}_{fV}$ = volume averaged FOSMOD factor

N_s = number of subison pore systems

P_c = capillary pressure, M/LT^2

S_{of} = final oil saturation

S_{or} = residual oil saturation from APEX

V = volume, L^3

V_p = pore volume of the core sample, L^3

V_{si} = volume of the *i*th subison pore system, L^3

Subscripts

1 = maximum

2 = minimum

References

Aggelopoulos, C. A., and Tsakiroglou, C. D. 2009. A Multi-Flowpath Model for the Interpretation of Immiscible Displacement Experiments in Heterogeneous Soil Columns. *Journal of Contaminant Hydrology*, **105**(3–4): 146–160. https://doi.org/10.1016/j.jconhyd.2008.12.004

Armstrong, R. T., and Berg, S. 2013. Interfacial Velocities and Capillary Pressure Gradients During Haines Jumps. *Physical Review E*, **88**(4): 043010. https://doi.org/10.1103/PhysRevE.88.043010

Armstrong, R. T., Georgiadis, A., Ott, H., Klemin, D., and Berg, S. 2014a. Critical Capillary Number: Desaturation Studied with Fast X-ray Computed Microtomography, *Geophysical Research Letters*, **41**(1): 55–60. https://doi.org/10.1002/2013GL058075

Armstrong, R. T., Ott, H., Georgiadis, A., Rücker, M., Schwing, A., and Berg, S. 2014b. Subsecond Pore-scale Displacement Processes and Relaxation Dynamics in Multiphase Flow. *Water Resources Research*, **50**(12): 9162–9176. https://doi.org/10.1002/2014WR015858

Bachu, S. 2008. CO_2 Storage in Geological Media: Role, Means, Status and Barriers to Deployment. *Progress in Energy and Combustion Science*, **34(**2): 254-273. https://doi.org/10.1016/j.pecs.2007.10.001

Balcewicz, M., Siegert, M., Gurris, M., Ruf, M., Krach, D., Steeb, H., and Saenger, E. H. 2021. Digital Rock Physics: A Geological Driven Workflow for the Segmentation of Anisotropic Ruhr Sandstone. *Frontiers in Earth Science*, **9**:673753. https://doi.org/10.3389/feart.2021.673753

Berg, S., Ott, H., Klapp, S. A., Schwing, A., Neiteler, R., Brussee, N., Makurat, A., Leu, L., Enzmann, F., Schwarz, J.-O., Kersten, M., Irvine, S., and Stampanoni, M. 2013. Real-time 3D Imaging of Haines Jumps in Porous Media Flow. *Proceedings of the National Academy of Sciences*, **110**(10): 3755–3759. https://doi.org/10.1073/pnas.1221373110

Berg, S., Armstrong, R., Ott, H., Georgiadis, A., Klapp, S. A., Schwing, A., Neiteler, R., Brussee, N., Makurat, A., Leu, L., and Enzmann, F. 2014. Multiphase Flow in Porous Rock Imaged Under Dynamic Flow Conditions with Fast X-Ray Computed Microtomography. *Petrophysics* **55**(04): 304-312. SPWLA-2014-v55n4a3

Blunt, M. J. 2001. Flow in Porous Media—Pore-network Models and Multiphase Flow. *Current Opinion in Colloid & Interface Science*, **6(**3): 197-207. https://doi.org/10.1016/S1359-0294(01)00084-X

Brooks, C. S., and Purcell, W. R. 1952. Surface Area Measurements on Sedimentary Rocks. Presented at the Fall Meeting of the Petroleum Branch of AIME, Houston, Texas, USA, 1-3 October. SPE-222-G. https://doi.org/10.2118/222-G

Bryant, S., and Blunt, M. 1992. Prediction of Relative Permeability in Simple Porous Media. *Physical Review A*, **46**(4): 2004-2011. https://doi.org/10.1103/PhysRevA.46.2004

Bryant, S. L., Mellor, D. W., and Cade, C. A. 1993. Physically Representative Network Models of Transport in Porous Media. *AIChE Journal*, **39**(3): 387-396. https://doi.org/10.1002/aic.690390303

Bultreys, T., Singh, K., Raeini, A. Q., Ruspini, L. C., Øren, P.-E., Berg, S., Rücker, M., Bijeljic, B., and Blunt, M. J. 2020. Verifying Pore Network Models of Imbibition in Rocks Using Time-Resolved Synchrotron Imaging. *Water Resources Research*, **56**(6): e2019WR026587. https://doi.org/10.1029/2019WR026587

Burdine, N. 1953. Relative Permeability Calculations from Pore Size Distribution Data. *Journal of Petroleum Technology*, **5**(03): 71-78. SPE-225-G. https://doi.org/10.2118/225-G

Carman, P. C. 1937. Fluid Flow Through Granular Beds. *Transactions of the Institution of Chemical Engineers*, **15**: 150-166.

Celia, M. A., Reeves, P. C., and Ferrand, L. A. 1995. Recent Advances in Pore Scale Models for Multiphase Flow in Porous Media. *Reviews of Geophysics*, **33**(S2): 1049-1057. https://doi.org/10.1029/95RG00248

Cerepi, A., Humbert, L., and Burlot, R. 2000. Pore-Scale Complexity of a Calcareous Material by Time-Controlled Mercury Porosimetry. *Studies in Surface Science and Catalysis*, **128**(2000): 449–458. https://doi.org/10.1016/S0167-2991(00)80050-6

Cerepi, A., Humbert, L., and Burlot, R. 2002. Dynamics of Capillary Flow and Transport Properties in Porous Media by Time-controlled Porosimetry. *Colloids and Surfaces A: Physicochemical and Engineering Aspects*, **206**(1–3): 425–444. https://doi.org/10.1016/S0927-7757(02)00065-1

Chandler, R., Koplik, J., Lerman, K., and Willemsen, J. F. 1982. Capillary Displacement and Percolation in Porous Media. *Journal of Fluid Mechanics*, **119**: 249-267. https://doi.org/10.1017/S0022112082001335

Chatzis, I., and Rezaei, N. 2006. A New Method for Characterizing the Pore Structure Heterogeneities in Carbonate Core Samples. Presented at the International Symposium of the Society of Core Analysts, Trondheim, Norway, 12-16 September.

Chen, M., Dai, J., Liu, X., Kuang, Y., Qin, M., and Wang, Z. 2018. Contributions of Pore-throat Size Distribution to Reservoir Quality and Fluid Distribution from NMR and MIP in Tight Sandy Conglomerate Reservoirs. *Arabian Journal of Geosciences*, **12**(1): 9. https://doi.org/10.1007/s12517-018-4153-7

Chen, Q., and Song, Y.-Q. 2002. What is the Shape of Pores in Natural Rocks? *The Journal of Chemical Physics*, **116**(19), 8247-8250. https://doi.org/10.1063/1.1477183

Childs, E. C., and Collis-George, N. 1950. The Permeability of Porous Materials. *Proceedings of the Royal Society of London. Series A. Mathematical and Physical Sciences*, **201**(1066): 392-405. https://doi.org/10.1098/rspa.1950.0068

Choquette, P. W., and Pray, L. C. 1970. Geologic Nomenclature and Classification of Porosity in Sedimentary Carbonates. *AAPG Bulletin*, **54**(2): 207-250. https://doi.org/10.1306/5D25C98B-16C1-11D7-8645000102C1865D

Coles, M. E., Hazlett, R. D., and Muegge, E. L. 1998. Developments in Synchrotron X-ray Microtomography with Applications to Flow in Porous Media. *SPE Reservoir Evaluation & Engineering*, **1**(04): 288-296. SPE-50985-PA. https://doi.org/10.2118/50985-PA

Crawford, F. W., and Hoover, G. M. 1966. Flow of Fluids Through Porous Mediums. *Journal of Geophysical Research*, **71**(12): 2911–2917. https://doi.org/10.1029/JZ071i012p02911

Daniels, J.K., Myers, M.T., Hathon, L.A. 2023. Estimating Fractal Dimension as a Spatially Correlated Pore Structure Heterogeneity Measure from Rate-Controlled Capillary Pressure Curve. Presented at the SPE Annual Technical Conference and Exhibition, San Antonio, Texas, USA. 16-18 October, SPE-215147-MS. https://doi.org/10.2118/215147-MS

Donaldson, E.C., Kendall, R.F., Pavelka, E.A., and Crocker, M.E. 1980. Equipment and procedures for fluid flow and wettability tests of geological materials. Technical Report, Report No. DOE/BETC/IC-79/5, US DOE, Bartlesville, OK, USA (May 1980). https://www.osti.gov/biblio/5279717

Fatt, I., and Dykstra, H. 1951. Relative Permeability Studies. *Journal of Petroleum Technology*, **3**(09): 249-256. SPE-951249-G. https://doi.org/10.2118/951249-G

Gao, H., Li, T., and Yang, L. 2016. Quantitative Determination of Pore and Throat Parameters in Tight Oil Reservoir Using Constant Rate Mercury Intrusion Technique. *Journal of Petroleum Exploration and Production Technology*, **6**(2): 309–318. https://doi.org/10.1007/s13202-015-0186-6

Gaulier, C. 1971. Studying Vugular Rocks By-Constant-Rate Mercury Injection. Presented at the Fall Meeting of the Society of Petroleum Engineers of AIME, New Orleans, Louisiana, USA, 3-6, October. SPE-3612-MS. https://doi.org/10.2118/3612-MS

Gibbs, J. W. 1878. On the Equilibrium of Heterogeneous Substances. *American Journal of Science*, **3**(96): 441-458.

Golparvar, A., Zhou, Y., Wu, K., Ma, J., and Yu, Z. 2018. A Comprehensive Review of Pore Scale Modeling Methodologies for Multiphase Flow in Porous Media. *Advances in Geo-Energy Research*, **2**(4): 418-440. https://doi.org/10.26804/ager.2018.04.07

Gostick, J. T., Ioannidis, M. A., Fowler, M. W., and Pritzker, M. D. 2009. Characterization of the Capillary Properties of Gas Diffusion Media. In *Modeling and Diagnostics of Polymer Electrolyte Fuel Cells*, ed. C.-Y. Wang, U. Pasaogullari, Chap. 7, 225–254. New York, USA: Modern Aspects of Electrochemistry, Springer Link. https://doi.org/10.1007/978-0-387-98068-3_7

Gostick, J., Aghighi, M., Hinebaugh, J., Tranter, T., Hoeh, M. A., Day, H., Spellacy, B., Sharqawy, M. H., Bazylak, A., Burns, A., Lehnert, W. and Putz, A. 2016. OpenPNM: A Pore Network Modeling Package. *Computing in Science & Engineering*, **18**(4): 60–74. https://doi.org/10.1109/MCSE.2016.49

Gostick, J. T., Misaghian, N., Yang, J., and Boek, E. S. 2022. Simulating Volume-controlled Invasion of a Non-wetting Fluid in Volumetric Images Using Basic Image Processing Tools. *Computers & Geosciences*, **158**, 104978. https://doi.org/10.1016/j.cageo.2021.104978

Haines, W. B. 1930. Studies in the Physical Properties of Soil. V. The Hysteresis Effect in Capillary Properties, and the Modes of Moisture Distribution Associated Therewith. *The Journal of Agricultural Science*, **20**(1): 97–116. https://doi.org/10.1017/S002185960008864X

Heller, J. P. 1968. The Drying Through the Top Surface of a Vertical Porous Column1. *Soil Science Society of America Journal*, **32**(6): 778-786. https://doi.org/10.2136/sssaj1968.03615995003200060024x

Hilfer, R. and Øren, P.-E. 1996. Dimensional Analysis of Pore Scale and Field Scale Immiscible Displacement. *Transport in Porous Media*, **22**: 53–72. https://doi.org/10.1007/BF00974311

Katz, A.J. and Thompson, A.H. 1986. Quantitative Prediction of Permeability in Porous Rock. *Physical Review B*, **34**(11): 8179-8181. https://doi.org/10.1103/PhysRevB.34.8179

Knackstedt, M. A., Sheppard, A. P., and Pinczewski, W. V. 1998. Simulation of Mercury Porosimetry on Correlated Grids: Evidence for Extended Correlated Heterogeneity at the Pore Scale in Rocks. *Physical Review E*, **58**(6): R6923–R6926. https://doi.org/10.1103/PhysRevE.58.R6923

Knackstedt, M. A., Sheppard, A. P., and Sahimi, M. 2001. Pore Network Modelling of Two-phase Flow in Porous Rock: The Effect of Correlated Heterogeneity. *Advances in Water Resources*, **24**(3-4): 257-277. https://doi.org/10.1016/S0309-1708(00)00057-9

Koplik, J. 1982. Creeping Flow in Two-dimensional Networks. *Journal of Fluid Mechanics*, ***119***: 219-247. https://doi.org/10.1017/S0022112082001323

Kozeny, J. 1927. Über Kapillare Leitung des Wassers im Boden. *Sitzungsberichte der Akademie der Wissenschaften in Wien* **136**: 271-306.

Laplace, P. S. 1807. *Supplément au Dixième Livre du Traité de Mécanique Céleste: A La Théorie de L'Action Capillaire*. Vol. 5. Chez J.B.M. Duprat, Libraire pour les Mathématiques, quai des Augustins. https://doi.org/10.5479/sil.338664.39088005644752

Lenormand, R., Zarcone, C., and Sarr, A. 1983. Mechanisms of the Displacement of One Fluid by Another in a Network of Capillary Ducts. *Journal of Fluid Mechanics*, **135**: 337-353. https://doi.org/10.1017/S0022112083003110

Lerdahl, T. R., Øren, P.-E., and Bakke, S. 2000. A Predictive Network Model for Three-phase Flow in Porous Media. Presented at the SPE/DOE Improved Oil Recovery Symposium, Tulsa, Oklahoma, 3-5 April. SPE-59311-MS. https://doi.org/10.2118/59311-MS

Lin, W., Wu, Z., Li, X., Yang, Z., Hu, M., Han, D., Wang, C., and Zhang, J. 2022. Digital Characterization and Fractal Quantification of the Pore Structures of Tight Sandstone at Multiple Scales. *Journal of Petroleum Exploration and Production Technology*, **12**: 2565-2575. https://doi.org/10.1007/s13202-022-01502-4

Liu, J., Song, S., Cao, X., Meng, Q., Pu, H., Wang, Y., and Liu, J. 2020. Determination of Full-scale Pore Size Distribution of Gaomiaozi Bentonite and its Permeability Prediction. *Journal of Rock Mechanics and Geotechnical Engineering*, **12**(2): 403–413. https://doi.org/10.1016/j.jrmge.2019.12.005

Mahmud, W. 1998. *Constant Rate Mercury Porosimetry to Characterize Pore Space Morphology*. M.S Thesis, University of New South Wales Sydney, Sydney, Australia (1988). https://doi.org/10.26190/unsworks/5456

Mahmud, W. 2022. Rate-Controlled Mercury Injection Experiments to Characterize Pore Space Geometry of Berea Sandstone. Presented at the International Symposium of the Society of Core Analysts. https://doi.org/10.1051/e3sconf/202336601016

Masalmeh, S. K., Jing., X., Roth, S., Wang, C., Dong, H., and Blunt, M. 2015. Towards Predicting Multiphase Flow in Porous Media Using Digital Rock Physics: Workflow to Test the Predictive Capability of Pore-Scale Modeling. Paper presented at the Abu Dhabi International Petroleum Exhibition and Conference, Abu Dhabi, UAE, 9-12, November. SPE-177572-MS. https://doi.org/10.2118/177572-MS

Mason, G. 1991. Discussion of Pore-scale Heterogeneity from Mercury Porosimetry Data. *SPE Formation Evaluation* **6**(02): 241. https://doi.org/10.2118/19617-PA

Meakin, P., and Tartakovsky, A. M. 2009. Modeling and Simulation of Pore-scale Multiphase Fluid Flow and Reactive Transport in Fractured and Porous Media. *Reviews of Geophysics*, **47**(3). https://doi.org/10.1029/2008RG000263

Melrose, J. C. 1965. Wettability as Related to Capillary Action in Porous Media. *SPE Journal*, **5**(03), 259–271. SPE-1085-PA. https://doi.org/10.2118/1085-PA

Melrose, J. C. 1970. Interfacial Phenomena as Related to Oil Recovery Mechanisms. *The Canadian Journal of Chemical Engineering*, **48**(6): 638-644. https://doi.org/10.1002/j.1939-019X.1970.tb00007.x

Melrose, J. C., and Brandner, C.F. 1974. Role of Capillary Forces in Determining Microscopic Displacement Efficiency for Oil Recovery by Waterflooding. *Journal of Canadian Petroleum Technology*, **13**(04): 54-62. PETSOC-74-04-05. https://doi.org/10.2118/74-04-05

Meng, Z., Sun, W., Liu, Y., Luo, B., and Zhao, M. 2021. Effect of Pore Networks on the Properties of Movable Fluids in Tight Sandstones from the Perspective of Multi-techniques. *Journal of Petroleum Science and Engineering*, ***201***: 108449. https://doi.org/10.1016/j.petrol.2021.108449

Miller, E. E., and Miller, R. D. 1956. Physical Theory for Capillary Flow Phenomena. *Journal of Applied Physics*, **27**(4), 324–332. https://doi.org/10.1063/1.1722370

Modrý, S., Svatá, M., and Van Brakel, J. 1981. Thematic Bibliography of Mercury Porosimetry. *Powder Technology*, **29**(1): 13-43. https://doi.org/10.1016/0032-5910(81)85002-4

Morrow, N. R. 1970. Physics and Thermodynamics of Capillary Action in Porous Media. *Industrial & Engineering Chemistry*, *62*(6), 32–56. https://doi.org/10.1021/ie50726a006

Moura, M., Måløy, K. J., and Toussaint, R. 2017. Critical Behavior in Porous Media Flow. *Europhysics Letters*, **118**(1): 14004. https://doi.org/10.1209/0295-5075/118/14004

Myers, M. T. 1991. Pore Combination Modeling: A Technique for Modeling the Permeability and Resistivity Properties of Complex Pore Systems. Presented at the SPE Annual Technical Conference and Exhibition, Dallas, Texas, USA, 6-9, October. SPE-22662-MS. https://doi.org/10.2118/22662-MS

Øren, P.-E., Bakke, S., and Arntzen, O. J. 1998. Extending Predictive Capabilities to Network Models. *SPE Journal*, **3**(04): 324-336. SPE-52052-PA. https://doi.org/10.2118/52052-PA

Purcell, W. R. 1949. Capillary Pressures - Their Measurement Using Mercury and the Calculation of Permeability Therefrom. *Journal of Petroleum Technology*, **1**(02): 39-48. SPE-949039-G. https://doi.org/10.2118/949039-G

Peters, E. J. 2012. *Advanced Petrophysics: Dispersion, Interfacial Phenomena/Wettability, Capillarity/Capillary Pressure, Relative Permeability*, First Edition, Vol. 2., Chapter 7, pp. 129, Live Oak Book Company, Austin, Texas .

Ren, D., Li, R., Liu, D., Li, Y., Liu, N., and Yang, F. 2019. Quantifying Fractal Dimension in Integrated Experimental Data of Tight Sandstones. *Geofluids*, **2019:** 6463473. https://doi.org/10.1155/2019/6463473

Rezaei, N., and Chatzis, I. 2011. Characterization of Heterogeneities in Porous Media Using Constant Rate Air Injection Porosimetry. *Journal of Petroleum Science and Engineering*, **79**(3–4): 113–124. https://doi.org/10.1016/j.petrol.2011.08.019

Ruspini, L. C., Øren, P.-E., Berg, S., Masalmeh, S., Bultreys, T., Taberner, C., Sorop, T., Marcelis, F., Appel, M., Freeman, J., and Wilson, O. B. 2021. Multiscale Digital Rock Analysis for Complex Rocks. *Transport in Porous Media*, **139**(2): 301-325. https://doi.org/10.1007/s11242-021-01667-2

Ruzyla, K. 1986. Characterization of Pore Space by Quantitative Image Analysis. *SPE Formation Evaluation*, **1**(04): 389-398. SPE-13133-PA. https://doi.org/10.2118/13133-PA

Siddiqui, S., Grader, A.S., Touati, M., Loermans, A.M. and Funk, J. J. 2005. Techniques for Extracting Reliable Density and Porosity Data from Cuttings. Presented at the SPE Annual Technical Conference and Exhibition, Dallas, Texas, USA, 9-12 October. SPE-96918-MS. https://doi.org/10.2118/96918-MS

Singh, K., Menke, H., Andrew, M., Lin, Q., Rau, C., Blunt, M. J., and Bijeljic, B. 2017a. Dynamics of Snap-off and Pore-filling Events During Two-phase Fluid Flow in Permeable Media. *Scientific Reports*, **7**(1): 5192. https://doi.org/10.1038/s41598-017-05204-4

Singh, K. 2017b. Movie_S3_Residual_Oil_Ganglia_after_Waterflooding.avi.figshare. Media. https://doi.org/10.6084/m9.figshare.4232324.v1

Singh, K., Menke, H., Andrew, M., Rau, C., Bijeljic, B., and Blunt, M. J. 2018a. Time-resolved Synchrotron X-ray Micro-tomography Datasets of Drainage and Imbibition in Carbonate Rocks. *Scientific Data*, **5**(1): 180265. https://doi.org/10.1038/sdata.2018.265

Singh, K. 2018b: Drainage in Carbonate Rocks: High-Resolution Time-Resolved Synchrotron X-Ray Micro-Tomography. figshare. Media. https://doi.org/10.6084/m9.figshare.7082885.v1

Singh, K. 2018c: Imbibition in Carbonate Rocks: High-resolution Time-resolved Synchrotron X-ray Micro-tomography. figshare. Media. https://doi.org/10.6084/m9.figshare.7082900.v1

Slichter, C. S. 1899. Theoretical Investigation of the Motion of Ground Waters. *US Geophysical Survey 19th Annual Report, Part II.*, 295-384. https://doi.org/10.3133/ar19_2

Smith, J.D., Chatzis, I., and Ioannidis, M.A. 2005. A New Technique to Measure the Breakthrough Capillary Pressure. *Journal of Canadian Petroleum Technology*, **44**(11): 25-31. PETSOC-05-11-01. https://doi.org/10.2118/05-11-01

Sorbie K.S., Wu Y.Z. and McDougall S.R. 1995. The Extended Washburn Equation and its Application to the Oil/Water Pore Doublet Problem. *Journal of Colloid and Interface Science*, **174**(2): 289 – 301. https://doi.org/10.1006/jcis.1995.1394

Spurin, C., Rücker, M., Moura, M., Bultreys, T., Garfi, G., Berg, S., Blunt, M.J. and Krevor, S. 2022. Red Noise in Steady-state Multiphase Flow in Porous Media. *Water Resources Research*, **58** (7): e2022WR031947. https://doi.org/10.1029/2022WR031947

Swanson, B.F. 1979. Visualizing Pores and Non-wetting Phase in Porous Rock. *Journal of Petroleum Technology*, **31**(01): 10–18. SPE-6857-PA. https://doi.org/10.2118/6857-PA

Swanson, B. F. 1981. A Simple Correlation Between Permeabilities and Mercury Capillary Pressures. *Journal of Petroleum Technology*, **33**(12): 2498-2504. SPE-8234-PA. https://doi.org/10.2118/8234-PA

Swanson, B. F. 1985. Microporosity in Reservoir Rocks: Its Measurement and Influence on Electrical Resistivity. *The Log Analyst*, **26** (06). SPWLA-1985-vXXVln6a3

Sygouni, V., Tsakiroglou, C. D., and Payatakes, A. C. 2006. Capillary Pressure Spectrometry: Toward a New Method for the Measurement of the Fractional Wettability of Porous Media. *Physics of Fluids*, **18**(05): 053302. https://doi.org/10.1063/1.2203667

Thomeer, J. H. 1983. Air Permeability as a Function of Three Pore-network Parameters. *Journal of Petroleum Technology*, **35**(04): 809-814. SPE-10922-PA. https://doi.org/10.2118/10922-PA

Thompson, A. H., Katz, A. J., and Krohn, C. E. 1987. The Microgeometry and Transport Properties of Sedimentary Rock. *Advances in Physics*, **36**(5): 625–694. https://doi.org/10.1080/00018738700101062

Toledo, P. G., Scriven, L. E., and Davis, H. T. 1994. Pore-Space Statistics and Capillary Pressure Curves from Volume-Controlled Porosimetry. *SPE Formation Evaluation*, **9**(01): 46-54. SPE-19618-PA. https://doi.org/10.2118/19618-PA

Tsang, Y. W., and Hale, F. V. 1998. A Study of the Application of Mercury Porosimetry Method to a Single Fracture. **23**.

Van Brakel, J., Modrý, S., and Svatá, M. 1981. Mercury Porosimetry: State of the Art. *Powder Technology*, **29**(1): 1-12. https://doi.org/10.1016/0032-5910(81)85001-2

Wang, X., Hou, J., Song, S., Wang, D., Gong, L., Ma, K., Liu, Y., Li, Y., and Yan, L. 2018. Combining Pressure-controlled Porosimetry and Rate-controlled Porosimetry to Investigate the Fractal Characteristics of Full-range Pores in Tight Oil Reservoirs. *Journal of Petroleum Science and Engineering*, **171**: 353–361. https://doi.org/10.1016/j.petrol.2018.07.050

Wang, F., and Zeng, F. 2020. Novel Insights into the Movable Fluid Distribution in Tight Sandstones Using Nuclear Magnetic Resonance and Rate-controlled Porosimetry. *Natural Resources Research*, **29**(5): 3351–3361. https://doi.org/10.1007/s11053-020-09635-1

Washburn, E. W. 1921a. Note on a Method of Determining the Distribution of Pore Sizes in a Porous Material. *Proceedings of the National Academy of Sciences*, **7**(4): 115-116. https://doi.org/10.1073/pnas.7.4.115

Washburn, E. W. 1921b. The Dynamics of Capillary Flow. *Physical Review*, **17**(3): 273-283. https://doi.org/10.1103/PhysRev.17.273

Bruce, W.A, and Welge, H.J. 1947. A Restored-State Method for Determination of Oil in Place and Connate Water. *API Drilling and Production Practice*, 161-165.

Wu, H., Zhang, C., Ji, Y., Liu, R., Cao, S., Chen, S., Zhang, Y., Wang, Y., Du, W., and Liu, G. 2018a. Pore Throat Characteristics of Tight Sandstone of Yanchang Formation in Eastern Gansu, Ordos Basin. *Petroleum Research*, **3**(1): 33–43. https://doi.org/10.1016/j.ptlrs.2017.11.001

Wu, H., Zhang, C., Ji, Y., Liu, R., Wu, H., Zhang, Y., Geng, Z., Zhang, Y., and Yang, J. 2018b. An Improved Method of Characterizing the Pore Structure in Tight Oil Reservoirs: Integrated NMR and Constant-Rate-controlled Porosimetry Data. *Journal of Petroleum Science and Engineering*, **166**: 778–796. https://doi.org/10.1016/j.petrol.2018.03.065

Xi, K., Cao, Y., Haile, B. G., Zhu, R., Jahren, J., Bjørlykke, K., Zhang, X., and Hellevang, H. 2016. How Does the Pore-Throat Size Control the Reservoir Quality and Oiliness of Tight Sandstones? The Case of the Lower Cretaceous Quantou Formation in the Southern Songliao Basin, China. *Marine and Petroleum Geology*, **76**: 1–15. https://doi.org/10.1016/j.marpetgeo.2016.05.001

Xiao, D., Jiang, S., Thul, D., Huang, W., Lu, Z., and Lu, S. 2017. Combining Rate-controlled Porosimetry and NMR to Probe Full-range Pore Throat Structures and Their Evolution Features in Tight Sands: A Case Study in the Songliao Basin, China. *Marine and Petroleum Geology*, **83**: 111–123. https://doi.org/10.1016/j.marpetgeo.2017.03.003

Xiao, D., Lu, S., Lu, Z., Huang, W., and Gu, M. 2016. Combining Nuclear Magnetic Resonance and Rate-controlled Porosimetry to Probe the Pore-throat Structure of Tight Sandstones. *Petroleum Exploration and Development*, **43**(6): 1049–1059. https://doi.org/10.1016/S1876-3804(16)30122-7

Xiao, D., Lu, Z., Jiang, S., and Lu, S. 2016. Comparison and Integration of Experimental Methods to Characterize the Full-range Pore Features of Tight Gas Sandstone—A Case Study in Songliao Basin of China. *Journal of Natural Gas Science and Engineering*, **34**: 1412–1421. https://doi.org/10.1016/j.jngse.2016.08.029

Xie, C and Guan, Z.. 2019. Study on 3D Micro-pore Structure Characteristics of Dolomite Reservoir with Different Scales. *Insights in Mining Science & Technology*, **1**(03). https://doi.org/10.19080/IMST.2019.01.555565

Yao, Y., and Liu, D. 2012. Comparison of low-field NMR and mercury intrusion porosimetry in characterizing pore size distributions of coals. *Fuel*, **95**: 152–158. https://doi.org/10.1016/j.fuel.2011.12.039

Young, T. 1805. III. An Essay on the Cohesion of Fluids. *Philosophical Transactions of the Royal Society*, **95**: 65-87. https://doi.org/10.1098/rstl.1805.0005

Yuan, H. H. 1991a. Pore-Scale Heterogeneity from Mercury Porosimetry Data. *SPE Formation Evaluation*, **6**(02): 233–240. https://doi.org/10.2118/19617-PA

Yuan, H.H. 1991b. Advances in Apex Technology: Determination of Cementation Exponent and Absolute Permeability. *The Log Analyst*, **32**(05). SPWLA-1991-v32n5a7.

Yuan, H. H., and Swanson, B. F. 1989. Resolving Pore-Space Characteristics by Rate-Controlled Porosimetry. *SPE Formation Evaluation*, **4**(01): 17–24. https://doi.org/10.2118/14892-PA

Zhang, W., Shi, Z., and Tian, Y. 2020. An Improved Method to Characterize the Pore-throat Structures in Tight Sandstone Reservoirs: Combined High-pressure and Rate-controlled Mercury Injection Techniques. *Energy Exploration & Exploitation*, **38**(6): 2389–2412. https://doi.org/10.1177/0144598720920729

Zhao, H., Ning, Z., Wang, Q., Zhang, R., Zhao, T., Niu, T., and Zeng, Y. 2015a. Petrophysical Characterization of Tight Oil Reservoirs Using Pressure-Controlled Porosimetry Combined with Rate-Controlled Porosimetry. *Fuel*, **154**: 233–242. https://doi.org/10.1016/j.fuel.2015.03.085

Zhao, H., Ning, Z., Zhao, T., Che, F., Zhang, R., and Hou, T. 2015b. Applicability Comparison of Nuclear Magnetic Resonance and Mercury Injection Capillary Pressure in Characterisation Pore Structure of Tight Oil Reservoirs. Presented at the SPE Asia Pacific Unconventional Resources Conference and Exhibition, Brisbane, Australia, 9-11 November, SPE-177026-MS. https://doi.org/10.2118/177026-MS

Zhao, H., Ning, Z., Zhao, T., Yu, L., Zhang, R., Dou, X., and Hou, T. 2015c. Geological and Petrophysical Characterization of Tight Oil Reservoirs: A Case Study from Upper Triassic Yanchang Formation, Ordos Basin in North China. Presented at the SPE Asia Pacific Unconventional Resources Conference and Exhibition, Brisbane, Australia, 9-11 November. SPE-177012-MS. https://doi.org/10.2118/177012-MS

Zhao, X., Yang, Z., Lin, W., Xiong, S., and Wei, Y. 2018. Characteristics of Microscopic Pore-throat Structure of Tight Oil Reservoirs in Sichuan Basin Measured by Rate-controlled Mercury Injection. *Open Physics*, **16**(1): 675–684. https://doi.org/10.1515/phys-2018-0086

Zhao, X., Yang, Z., Lin, W., Xiong, S., Luo, Y., Wang, Z., Chen, T., Xia, D., and Wu, Z. 2019. Study on Pore Structures of Tight Sandstone Reservoirs Based on Nitrogen Adsorption, High-Pressure Mercury Intrusion, and Rate-Controlled Mercury Intrusion. *Journal of Energy Resources Technology*, **141**(11): 112903. https://doi.org/10.1115/1.4043695